Response of Duplex Cr(N)/S and Cr(C)/S Coatings on 316L Stainless Steel to Tribocorrosion in 0.89% NaCl Solution Under Plastic Contact Conditions

Y. Sun[1*], P.A. Dearnley[2], Bertram Mallia[3]

1 School of Engineering and Sustainable Development, Faculty of Technology, De Montfort University, Leicester LE1 9BH, UK. Email: ysun01@dmu.ac.uk
* Corresponding author

2 Boride Services Ltd, Leeds, UK

3 Faculty of Engineering, University of Malta, Msida Campus, MSD 2080

Abstract

Two duplex coatings, Cr(N)/S and Cr(C)/S, were deposited on 316L stainless steel by magnetron sputtering. The effectiveness of these duplex coatings in improving the tribocorrosion behaviour of medical alloys under elastic contact conditions has been demonstrated in a recent publication. The present work focused on the response of these duplex coatings to tribocorrosion under plastic contact conditions. Tribocorrosion tests were conducted in 0.89 % NaCl solution at 37^{o}C at an initial contact pressure of 740 MPa and under unidirectional sliding conditions for sliding duration up to 24 h. The results showed that during sliding in the corrosive solution, the duplex coatings were plastically deformed into the substrate to a depth about 1 μm. The Cr(C)/S duplex coating had sufficient ductility to accommodate the deformation without cracking, such that it was worn through gradually, leading to the gradual increase in open circuit potential (OCP) and coefficient of friction (COF). On the other hand, the Cr(N)/S duplex coating suffered from cracking at all tested potentials, leading to coating blistering after prolonged sliding at OCP and stable pit formation in the substrate beneath the coating at applied anodic potentials.

Keywords: Stainless steel; Tribocorrosion; Coating; Friction; Wear

1 Introduction

It has been recognized that tribocorrosion or corrosion-wear plays an important role in material degradation in tribological systems exposed to corrosive environments [1-3]. The combined chemical and mechanical actions can lead to the synergism between wear and corrosion, resulting in wear-accelerated corrosion and corrosion-accelerated wear [4,5]. In biomedical systems, such as in artificial prostheses, the load bearing/articulating surfaces are lubricated by the hostile corrosive body fluids, forming a typical tribocorrosion system which not only suffers from accelerated material loss and the generation of wear particles around the joint area, but also leads to the release of metal ions [6]. There have been increasing concerns regarding the long term durability of the joint replacement due to the generation of nano-sized particles and the release of toxic metal ions [7,8]. Thus, many efforts have been made in the past decade to investigate the tribocorrosion behaviour of biomedical alloys in laboratory and simulator tests [9-12]. One of the ways to improve the tribocorrosion properties of metallic alloys is by forming a barrier layer at the surface through surface engineering, in particular by applying hard and corrosion resistant coatings [13,14].

Indeed, many efforts have been made to improve the tribocorrosion performance of biodemical alloys by surface coatings, including diamond-like carbon coatings [15], ion implantation [16], TiN and TiC based coatings [17], CrN based coatings [18] and surface alloying [19,20]. In particular, detailed studies have been performed on the potential of S-phase coating and CrN coating to improve the tribocorrosion behaviour of biomedical alloys [21,22]. S-phase coating is an austenitic stainless steel or CoCr alloy coating supersaturated with nitrogen or carbon, possessing a high hardness (>800 Hv) and good corrosion resistance [21,23]. The S-phase was initially produced by low temperature nitriding or carburizing of austenitic stainless steels and CoCr alloys with a face-centred cubic structure [24,25]. By magnetron sputtering a stainless steel or CoCrMo alloy target in the presence of nitrogen or carbon containing atmospheres, S-phase

coatings can be fabricated [21-23]. A Cr(N) or Cr(C) coating can be further deposited on top of the S-phase coating to produce a duplex coating system on biomedical alloys [23].

In previous work on duplex Cr(N)/S and Cr(C)/S coatings on CoCrMo alloy, the effectiveness of these coating systems in improving the tribocorrosion behaviour of the biomedical alloy under elastic contact conditions has been demonstrated [23]. In practical applications, engineering components are normally designed within the elastic limit. In a typical hip and knee joint, the maximum contact pressure has been reported to be below 60 MPa, which is well within the elastic limit of such biomedical alloys as titanium, stainless steel and CoCrMo [26]. It is thus essential that the coating-substrate system should be tested under elastic contact conditions. However, there are concerns regarding the sustainability of the coating system subjected to progressive material loss under tribocorrosion conditions, arising from the limited coating thickness, coating adhesion and the difference in electrochemical potential between the coating and substrate materials. Such concerns become more obvious when localized damage occurs to the coating after prolonged sliding and due to localized plastic deformation caused by trapped wear particles or surface asperities. It has been known that plastic deformation can change the electrochemical response of the material during tribocorrosion [27]. It is thus important to have an understanding of the response of the coating-substrate system to tribocorrosion after prolonged sliding contact and under more severe loading conditions when the coating is gradually worn through and/or suffers from localized damage due to plastic deformation and cracking. This requires prolonged laboratory testing under controlled loading and electrochemical conditions and forms the main theme of the present work.

In the present work, magnetron sputtering was used to deposit two types of duplex coatings, Cr(N)/S and Cr(C)/S, onto AISI 316L stainless steel. The aim of this work was to evaluate the response of these duplex coatings to tribocorrosion under plastic contact conditions during prolonged sliding when the coating were worn through and suffered from localized damage.

2 Materials and Methods

The substrate material used was AISI 316L stainless steel which had the following nominal composition (in wt.%): 0.02C, 18.61Cr, 11.83Ni, 2.87Mo, 2.1Mn, 0.76Si, 0.045P, 0.03S and balance Fe. Specimens of 20 mm x 20 mm x 2 mm were machined from a hot-rolled plate. The surface to be coated was ground using progressively finer SiC grinding papers and then finished by 1 micron diamond polishing to achieve a surface finish of 0.02 μm (R_a). Prior to coating deposition, the specimens were cleaned ultrasonically in acetone for 10 minutes.

A laboratory scale magnetron sputtering machine was used to produce the duplex coatings. Details of the deposition procedures have been described elsewhere [23]. Briefly, an interfacial layer about 0.25 μm thick was first applied to the substrates by sputtering a CoCrMo target in argon plasma. This was followed by the deposition of the inner carbon S-phase sublayer about 2.0 μm thick, achieved by sputtering the CoCrMo target in an atmosphere prepared by flowing a mixture of Ar and CH_4 into the chamber. Finally a top layer of Cr(N) or Cr(C) about 1.4 μm thick was deposited by sputtering a pure Cr target in atmospheres respectively containing a mixture of Ar and N_2 or Ar and CH_4. Table 1 summarizes the characteristics of the duplex coatings as characterised by energy dispersion X-ray (EDX) composition analysis, X-ray diffraction (XRD), layer thickness measurements and nanoindentation tests. It was noted that the Cr(N) coating had a crystalline fcc structure while the Cr(C) coating was amorphous since no diffraction peaks were detected by XRD. As shown in Table 1, the Cr(N)/S coating was harder and stiffer than the Cr(C)/S coating.

All corrosion and tribocorrosion tests here were conducted at 37^{o}C in physiological saline (0.89%NaCl) solution, which is often chosen as baseline medium for testing coated metal implant alloys, to represent the salinity level found in the human body [28-30]. It is recognised that saline-bovine serum solutions can also be used since these are widely used in human joint simulator tests [14] due to their ability to reproduce the lower friction levels found in human joints.

However, for the purposes of achieving a first-level ranking of coated biomedical metals, physiological saline is a pragmatic choice. Once suitable candidate coating/substrate materials have been identified, more advanced simulator tests (using saline-bovine serum solutions at 37°C) can be carried out.

Anodic polarization tests were initially carried out without sliding to assess the electrochemical corrosion behaviour of the specimens. These were conducted using a three-electrode setup, where the specimen was the working electrode, a Saturated Calomel Electrode (SCE) served as the reference electrode and a platinum wire was the auxiliary electrode. To standardize and clean the surface, the specimens were cathodically polarized at -600 mV(SCE) for 180 s and then rested (stabilized) at open circuit for 600 s. The evolution of open circuit potential (OCP) during the rest period was recorded continuously. Anodic polarization was then started from -200 mV(SCE) vs OCP at a scan rate of 1 mV s^{-1} until a current density of 1 mA cm^{-2} was reached. All the electrochemical measurements were realized using an ACM Gill AC potentiostat.

Tribocorrosion tests were conducted under unidirectional sliding by integrating a pin-on-disk tribometer with the potentiostat [31]. The sliding contact pin was an inert sintered alumina ball of 8 mm diameter. Prior to the test, the specimens were masked using insulating lacquer to leave a test area of 11 mm diameter exposed to the electrolyte. A Saturated Calomel Electrode (SCE) was inserted into the test cell containing 250 ml electrolyte to serve as the reference electrode and a platinum wire was used as the auxiliary electrode. All tests were conducted in open air at a temperature of 37^{o}C, controlled by an external heating reservoir.

All tribocorrosion tests were conducted at a rotating speed of 60 rpm under a constant load of 2 N applied to the Al_2O_3 ball. A contact load of 2 N was employed to ensure that some plastic deformation was induced in the 316L steel substrate, in line with the major objective of this work. Hertz elastic contact analysis indicated that the initial contact pressure was ~740 MPa for Al_2O_3 on uncoated 316L steel with a maximum shear stress of 231 MPa at a depth of 17 μm below the

surface. According to the Tresca criterion, such a maximum shear stress was sufficient to cause bulk plastic deformation of 316L stainless steel which has uniaxial and shear yield strengths about ~300 MPa and 150 MPa respectively. Thus plastic deformation in the substrate of the duplex coating systems was expected during tribocorrosion tests.

The first series of tests were conducted at OCP for various durations ranging from 1 h to 24 h. Further tests were also conducted at a cathodic potential of -700 mV(SCE) and an anodic potential of 100 mV(SCE) for a fixed duration of 3 h. Long test times at OCP were intentionally used to assess the response of the coating systems to tribocorrosion after the coating was locally damaged or worn through. In all tests, the corrosion-wear track diameter was 6 mm. Before sliding started, the specimen was standardized by cathodic polarizing at -600 mV(SCE) for 180 s, followed by resting at the test potential for 600 s. After sliding for the predetermined time, the specimen was rested at the test potential for further 600 s. The open circuit potential (or current) and coefficient of friction (COF) were recorded continuously before, during and after sliding. Each test was duplicated and the averaged results recorded.

After testing, a ball crater 0.5-1.0 mm diameter was made on each corrosion-wear track to provide a visual view of the wear depth and material deformation behaviour beneath the wear track. Fig 1 shows a typical ball crater made on the wear track on a duplex coated specimen. The actual wear depth in the wear track relative to the duplex coatings can be clearly seen. More importantly, it reveals that the coatings in the wear track were plastically deformed into the substrate, as evidenced by the deformation of the coatings beyond the original circular contours of the coating interfaces. The total material loss from each corrosion-wear track was evaluated by measuring the surface profile across the track using a contacting surface profilometer (Mitutoyo SJ400). The surface morphology of the corrosion-wear tracks were subsequently examined by optical microscope and scanning electron microscope (SEM) equipped with EDX and depth profile facilities.

3 Results

3.1 Corrosion behaviour without sliding

Experiments were first conducted to evaluate the electrochemical corrosion behaviour of the test specimens under static conditions without sliding. Fig. 2a shows the evolution of OCP with rest time after cathodic polarization at -600 mV(SCE) for 180 s. As expected, the OCP of all specimens increased with time due to the repassivation of the exposed surface and thickening of the passive film. At the early stage of exposure, the OCP of the uncoated surface developed much faster than those of the duplex coatings, although the latter reached higher OCP values than the former after 200 s. It is thus evident that after the removal or partially removal of the passive film by cathodic polarization, the uncoated surface repassivated faster than the duplex coatings. This may explain the larger cathodic drop in OCP of the duplex coatings during sliding, as discussed later.

The anodic polarization curves measured under the condition without sliding for the test specimens are shown in Fig. 2b. The uncoated surface was at the passive state at anodic potentials until pit formation at about 320 mV(SCE) as confirmed by the sharp rise in current density and by microscopic examination of the corroded surface. The duplex coatings showed very low anodic current densities which were two orders of magnitude lower than those from the uncoated specimen. The increase in current density at potentials above 700 mV(SCE) was presumably due to transpassivity and oxygen evolution. Among the two duplex coatings, the Cr(N)/S coating exhibited the lowest anodic dissolution rates and the best corrosion resistance.

3.2 Sliding at OCP for various times

The next series of experiments involved sliding at OCP for various times, from 1 h to 12 h for the uncoated specimen and the Cr(C)/S coated specimen and up to 24 h for the Cr(N)/S coated specimen. A longer test time was used for the latter because the top Cr(N) coating was not worn

through after 12 h sliding. Even after 24 h sliding, the top Cr(N) coating was not completely worn through, but suffered from localized failure due to blistering.

3.2.1 Electrochemical and frictional response

Fig. 3 shows the OCP and COF recorded during the test. Two representative OCP and COF curves for two different sliding times are presented for each specimen. At the beginning of sliding, the drop in OCP was more significant for the coated specimens than for the uncoated specimen (Fig. 3a). This could be explained by the faster repassivation of the uncotated surface as evidenced in Fig. 2a. During sliding, the OCP of the uncoated specimen continued to decrease with time (Fig. 3a) due to increased wear track area [5,32], which was accompanied with high COF values around 0.6 with large frictional noises (Fig. 3b). On the other hand, the OCP of the coated specimens increased with sliding time (Fig. 3a). The OCP of the Cr(C)/S coated specimen initially increased slowly and smoothly with sliding time and experienced a sharp rise after about 4 h sliding and then gradually reached the values for the uncoated specimen (Fig. 3a). Corresponding, the COF of the Cr(C)/S coated specimen showed low values between 0.25 and 0.35 for the first 4 h sliding and then increased with further sliding in both magnitude and noise level to reach the values characteristic of the uncoated specimen (Fig. 3b). Fig. 4a shows the wear track profiles measured by profilometer. It can be seen that during sliding for 3 h, wear mainly occurred within the top Cr(C) coating with only a deep scratch penetrating through the Cr(C) coating to reach the S-phase sublayer. After sliding for 6 h, the top Cr(C) coating was worn through and wear occurred within the S-phase sublayer. After 12 h sliding, both the top Cr(C) coating and the S-phase sublayer were worn through, leading to the exposure of the substrate and significant roughening of the worn surface and accelerated total material loss (TML). It is thus evident that the observed variation in OCP and COF with sliding time in Fig. 3 for the Cr(C)/S coated specimen was due to the gradual wearing through of the top Cr(C) coating and then the S-phase sublayer to expose the substrate.

Different electrochemical and frictional behaviour was observed for the Cr(N)/S coated specimen, which experienced a large scatter in OCP during sliding: the OCP followed a general trend of increasing with sliding time (Fig. 3a). As discussed later, this was associated with cracking of the top Cr(N) coating, leading to the exposure of the underlying S-phase layer and then the substrate to the electrolyte through the cracks. The duplex Cr(N)/S coated specimen exhibited the lowest friction throughout the whole test period of 24 h, which started to increase slightly after 12 h (Fig. 3b). Rather surprisingly, the COF of the Cr(N)/S coated specimen did not follow the same trend as the OCP, suggesting that the contact between the top Cr(N) coating and the slider dominated throughout the sliding process up to 24 h. Obviously, cracks in the coating did not significantly affect COF but affected OCP. Indeed, wear track profile measurements revealed that the top Cr(N) coating was not worn through after 12 h sliding and only experienced local failure after 24 h sliding (Fig. 4b).

3.2.2 Examination of ball crater on corrosion-wear track

Fig. 5 shows typical ball craters made on the corrosion-wear tracks on the Cr(C)/S coated specimen. In consistence with wear track profile measurement in Fig. 4a, wear mainly occurred in the top Cr(C) coating during sliding for 3 h. With continued sliding for 6 h, the top Cr(C) coating was worn through (Fig. 5b). Further extending the sliding time to 12 h led to the wearing through of the S-phase sublayer and the acceleration in total material loss. More importantly, the ball-cratering technique clearly revealed that the top Cr(C) coating and the S-phase sublayer in the wear track were plastically deformed beyond the original contours towards the substrate. Judging from the coating thickness, it was estimated that the deformation depth of the duplex coatings was about 1 μm. This observation provided direct evidence of plastic deformation of the coatings towards the substrate in the wear track in such a small scale.

Fig. 6 shows the ball craters made on the wear tracks on the Cr(N)/S coated specimen after sliding for various times. Again, several interesting observations can be made here. The top Cr(N)

coating was not worn through after 12 h sliding (Fig. 6b), but was worn through locally by some deep scratches after 24 h testing (Fig. 6c). In the wear track, the top Cr(N) coating and the S-phase sublayer were plastically deformed towards the substrate as evidenced by the deformation of the coatings beyond the original circular contours. Such plastic deformation in the wear track happened at the very beginning of the sliding process (1 h sliding, Fig. 6a). It is also interesting to note that deep scratches in the wear track resulted in deep deformation of the duplex coatings towards the substrate (Fig. 6a).

3.2.3 Surface morphology of corrosion-wear tracks

For the Cr(C)/S coated specimen, corrosion-wear of the top Cr(C) coating occurred in a smooth mode by micro-abrasion and polishing, as evidenced by the smooth and polished corrosion-wear track surface appearance observed in Fig. 5a after sliding for 3 h. After wearing through of the top Cr(C) coating, the wear mechanisms changed to severe abrasion, as shown in Fig. 5b for the corrosion-wear tracks after sliding for 6 h. In all corrosion-wear tracks on the Cr(C)/S coated specimen, no cracks were observed although the duplex coatings were plastically deformed towards the substrate as discussed above (see Fig. 5). This suggests that the top Cr(C) coating had sufficient ductility to accommodate the deformation of about 1 μm depth without cracking.

On the other hand, the most striking morphological feature observed on the corrosion-wear tracks on the Cr(N)/S coated specimen was cracking, as shown in Fig. 7. No coating wearing-through and debonding have been found after sliding for up to 12 h (Fig. 7c). Sliding for extended 24 h led to the formation of many shallow pits in the corrosion-wear track, due to blistering of the Cr(N) coating initiated at the cracks (Fig. 7d). More detailed examinations of the worn surfaces were made by SEM, coupled with EDX analysis and depth-profile measurements equipped with SEM (Fig. 8). Obviously, the cracks had sufficient openings to allow the electrolyte to penetrate into the subsurface (Fig. 8a and c), promoting localized corrosion. The typical depth of coating blistering after 24 h sliding was around 1.5 μm (Fig. 8c), thus it was the top Cr(N) coating which

flaked off, as further confirmed by EDX spot analysis and elemental mapping, which detected Co from the S-phase sublayer in the blistered areas. SEM examination of the edges of the ball craters made on the corrosion-wear tracks revealed details of the coatings beneath the corrosion-wear track (Fig. 8 b and d), providing direct evidence that cracks seen on the duplex coating surface were actually extended into the S-phase sublayer after 6 h sliding (Fig. 8b) and further into the substrate after 24 h sliding (Fig. 8d) at OCP.

3.2.4 Total material loss (TML)

TML from the corrosion-wear track was evaluated from the track profiles measured by profilometer (Fig. 4). The results are shown in Fig. 9 as a function of sliding time. It can be seen that the application of the duplex Cr(C)/S coating reduced the TML of 316L steel by more than 3 times even after the top Cr(C) coating was worn through after 6 h sliding.

Although cracks were formed in the wear track of the Cr(N)/S coated specimen, this duplex coating was the most effective in reducing TML, by nearly an order of magnitude as compared to that of the uncoated specimen (Fig. 9). This was because the Cr(N)/S duplex coating maintained its integrity with the substrate without debonding regardless of crack formation. The cracked duplex coating affected the evolution of OCP (Fig. 3a) but still provided protection to the steel against friction (Fig. 3b) and material loss (Fig. 9) within the time scale tested in this work. However, after prolonged sliding at OCP for 24 h, the cracks served as initiation sites for coating blistering, leading to the formation of shallow pits (Fig. 8).

3.3 Effect of applied potential

Further tests were conducted for a fixed sliding time of 3 h at a cathodic potential (CP) of -700 mV(SCE) and an anodic potential (AP) of 100 mV(SCE). The measured TML values are summarized in Fig. 10, from which it can be seen that the duplex Cr(N)/S coating exhibited the smallest TML at all potentials tested, while the duplex Cr(C)/S coating was effective in reducing TML of 316L steel at OCP and AP but not at CP.

At CP, since the measured currents were negative throughout the tests for all specimens, corrosion was not expected and TML was purely due to mechanical wear [5,31]. Thus smaller TML should be expected because of the absence of chemical wear and wear-corrosion synergism [1,3,5]. Indeed, at CP the TML from the uncoated specimen and from the Cr(N)/S coated specimen was reduced as compared to that tested at OCP (Fig. 10). However, the TML from the Cr(C)/S coated specimen was larger at CP than at OCP. Such an unusual behaviour of the Cr(C) coating at CP was also observed in a previous study on duplex coated CoCrMo alloy under elastic contact conditions and was attributed to the observed material transfer to the alumina slider [23]. As expected, at AP the TML from all specimens was increased due to the combined effects of wear and corrosion and their synergism, a phenomenon observed by many investigators for passive systems [3-5,9,10].

Fig. 11 shows the ball craters made on the corrosion-wear tracks on the Cr(C)/S coated specimen produced by sliding at CP and AP. Deformation of the duplex coatings into the substrate was evident at both CP and AP. Deeper scratches on the corrosion-wear track resulted in deeper deformation of the coating into the substrate. At both potentials, the top Cr(C) coating was not worn through in most areas of the corrosion-wear track, but rather deformed towards the substrate. In areas with deep scratches, the top Cr(C) coating was worn through locally. No cracks and no corrosion pits were observed in the corrosion-wear tracks at both potentials.

The surface morphology of the corrosion-wear tracks on the Cr(N)/S coated specimen produced at CP and AP had a polished appearance and cracks were formed in the track at both potentials (see Fig. 12a). Several stable pits of about 100 μm in size were also observed in the corrosion-wear track produced at AP (Fig. 12). These pits were developed in the substrate beneath the Cr(N) coating and the coating collapsed into the substrate during subsequent contact motion. Ball cratering revealed that corrosion-wear of the top Cr(N) coating was very small at both CP and AP (Fig. 13), but rather the Cr(N) coating and S-phase sublayer were deformed towards the

substrate at both potentials. After abrading away the top Cr(N) coating and the underlying S-phase sublayer, the pit initially seen on the corrosion-wear track surface (Fig. 12) can be clearly seen deep in the substrate (Fig. 13b).

4 Discussion

Two types of coatings were studied in this work. The Cr(N) coating had a crystalline structure and was harder and stiffer than the Cr(C) coating which had an amorphous structure. Under the present plastic contact conditions, a common feature observed for both duplex coatings was the plastic deformation of the coatings towards the substrate to a depth about 1 μm (Figs 5 and 6). Such deformation was independent of applied potential (Figs 11 and 13) and thus was purely a mechanical behaviour due to the relatively high contact stresses above the yield point of 316L steel. However, the response of these two coatings to the plastic deformation was different. The Cr(C)/S duplex coating had sufficient ductility to accommodate the plastic deformation without cracking and pit formation, such that the coating was worn through smoothly, leading to the gradual increase in OCP and COF during sliding under open circuit conditions. On the other hand, the Cr(N)/S duplex coating suffered from severe cracking at all applied potentials (Figs 7, 8 and 12). Although the Cr(N)/S coating maintained its integrity with the substrate without debonding and offered much reduced TML (Figs 9 and 10), the formation of cracks in the wear track had significant effect on the tribocorrosion behaviour of the duplex coating in several aspects, as discussed below.

Firstly, with increasing sliding time, the cracks propagated from the top Cr(N) coating through the S-phase sublayer to the substrate. This allowed for the electrolyte to penetrate to the subsurface, promoting localized corrosion and coating blistering after prolonged sliding at OCP (Fig. 8). Although this was not reflected in the TML measured by profilometer (Fig. 9), it would impose a serious concern regarding the sustainability of such a coating system in applications where plastic deformation of the substrate may be encountered.

Secondly, at the applied anodic potential, stable pits formed in the corrosion-wear track below the Cr(N)/S duplex coating, leading the collapse of the coating (Fig. 12). Fig. 14 shows the enlarged view of the edge of the ball crater in Fig. 13b, revealing details of the cracks in the corrosion-wear track. Most of the cracks continued from the worn surface through the Cr(N) coating into the S-phase sublayer to reach the substrate. These through-cracks could form ideal sites for localized corrosion of the substrate, promoting pit formation beneath the duplex coating even though 100 mV(SCE) was well below the pitting potential of the substrate 316L steel (320 mV(SCE)). The formation of pits at the substrate beneath the coating then would lead to the collapse of the coating.

The deformation, cracking and corrosion-wear behaviour of the duplex coatings at AP were also reflected in the recorded anodic current transients, shown in Fig. 15. For all specimens, the current increased significantly upon the commencement of sliding and continued to increase during sliding. Both Cr(C)/S and Cr(N)/S duplex coatings were effective in reducing anodic current during sliding as compared to the uncoated specimen, thus reducing chemical wear. For the Cr(C)/S coated specimen, the current initially increased smoothly with sliding time and then after about 1.8 h sliding experienced a large increase and large scattering, which could be explained by the localized wearing through of the top Cr(C) coating (Fig. 11b). For the Cr(N)/S coating, although the overall current was lower than that from the Cr(C)/S coating, the current showed an erratic behaviour with spikes from the early stage of sliding. Obviously, this erratic current transient behaviour was the result of crack formation in the corrosion-wear track. The electrolyte could penetrate the through-cracks (Fig. 14) to reach the substrate, resulting in localized metal dissolution from the substrate and the formation of pits beneath the Cr(N) coating as observed on the corrosion-wear track (Fig. 12 and Fig. 13b). It is also interesting to note that after the termination of sliding, the current from the uncoated specimen and the Cr(C)/S coated specimen was decreased quickly to reach the originally low level registered before sliding, suggesting

repassivation of the corrosion-wear track area and the absence of stable pit formation. However, the current from the Cr(N)/S coating did not decrease, but continued to increase with rest time at 100 mV without sliding. This was due to the stable pits formed in the corrosion-wear track during sliding, which continued to grow in size after the termination of sliding because the pits were covered with the Cr(N) coating which served as a diffusion barrier to prevent the solution in the pits from being diluted.

4 Conclusions

Based on the experimental results obtained under plastic contact conditions at OCP, CP and AP, several conclusions can be drawn regarding the response of the duplex coatings to tribocorrosion in the test solution at 37^{o}C.

(1) During tribocorrosion under the present plastic contact conditions, the duplex coatings are plastically deformed into the substrate. The deformation depth of the coatings is about 1 μm. Deep scratches in the corrosion-wear track result in deeper deformation of the duplex coatings.

(2) The Cr(C)/S duplex coating has sufficient ductility to accommodate the plastic deformation without cracking, such that the coating is worn through smoothly, leading to the gradual increase in OCP and COF during sliding under open circuit conditions.

(3) The Cr(N)/S duplex coating does not have sufficient ductility to accommodate the plastic deformation, such that cracks are formed on the corrosion-wear track surface. At OCP, crack formation in the Cr(N)/S duplex coating affects the evolution of OCP during sliding due to the exposure of the underlying S-phase and the substrate to the solution through the cracks. But COF is not affected by crack formation once the coating maintains its integrity with the substrate. However, with prolonged sliding at OCP, the cracks serve as initiation sites for coating blistering, leading to local failure of the Cr(N) coating.

(4) At AP, cracking of the Cr(N) coating leads to the exposure of the substrate to the solution through the cracks, promoting localized metal dissolution from the substrate and the formation of

stable pits in the substrate beneath the coating. This in turn leads to the collapse of the Cr(N) coating into the substrate in pitting areas.

(5) Under the present testing conditions, the Cr(N)/S duplex coating is the most effective in reducing TML, COF and chemical wear of 316L stainless at all applied potentials. But crack formation in the corrosion-wear track can lead to localized failure through coating blistering after prolonged sliding at OCP or through accelerated pit formation in the substrate beneath the coating in more aggressive environments (e.g. at AP). These impose serious concerns regarding the sustainability of the coating system in applications where plastic deformation of the substrate maybe encountered.

References

[1] Watson SW, Friedersdorf FJ, Madsen BW, Gramer SD, Methods of measuring wear-corrosion synergism, Wear 1995; 181-183: 476-484.

[2] Lemaire E, Le Calvar M, Evidence of tribocorrosion wear in pressurized water reactors, Wear 2001; 249: 338-344.

[3] Mischler S, Triboelectrochemical techniques and interpretation methods in tribocorrosion: A comparative evaluation, Tribology International 2008; 41: 573-583.

[4] Jiang J, Stack MM, Neville A, Modelling the tribo-corrosion interaction in aqueous sliding conditions, Tribology International 2002; 35: 669-679.

[5] Landolt D, Mischler S, Stemp M, Electrochemical methods in tribocorrosion: a critical appraisal, Electrochimica Acta 2001; 46: 3913-3929.

[6] Yolanda Hedberg, Inger Odnevall Wallinder, Metal release and speciation of released chromium from a biomedical CoCrMo alloy into simulated physiologically relevant solutions, Journal of Biomedical Materials Research Part B: Applied Biomaterials 2014; 102: 693-699.

[7] MacDonald SJ, Can a safe level for metal ions in patients with metal-on metal total hip arthroplasties be determined? Journal of Arthroplasty 2004; 19: 71–77.

[8] Germain MA, Hatton A, Williams S, Matthews JB, Stone MH, Fisher J, Ingham E, Comparison of the cytotoxicity of clinically relevant cobalt–chromium and alumina ceramic wear particles in vitro, Biomaterials 2003; 24: 469–479.

[9] Viswanathan Swaminathan, Jeremy L. Gilbert, Fretting corrosion of CoCrMo and Ti6Al4V interfaces, Biomaterials 2012; 33: 5487-5503.

[10] Stefano Mischler, Anna Igual Munoz, Wear of CoCrMo alloys used in metal-on-metal hip joints: a tribocorrosion appraisal, Wear 2013; 297: 1081-1094.

[11] Sadiq K, Stack MM, Black RA, Wear mapping of CoCrMo alloy in simulated bio-tribocorrosion conditions of a hip prosthesis bearing in calf serum solution, Materials Science and Engineering 2015; C49: 452-462.

[12] John KR, Zardiackas LD, Poggie RA, Wear evaluation of cobalt–chromium alloy for use in a metal-on-metal hip prosthesis, Journal of Biomedical Materials Research Part B: Applied Biomaterials 2004; 68B: 1-14.

[13] Wood RJK, Wharton JA, Coatings for tribocorrosion protection, in Landolt D and Mischler S (ed) Tribocorrosion of Passive Metals and Coatings 2011, Woodhead Publishing Limited, pp296-333.

[14] Leslie IJ, Williams S, Brown C, Anderson J, Isaac G, Hatto P, Ingham E and Fisher J, Surface engineering: A low wearing solution for metal-on-metal hip surface replacements, Journal of Biomedical Materials Research Part B: Applied Biomaterials 2009; 90B: 558-565.

[15] Ritwik Kumar Roy, Kwang-Ryeol Lee, Biomedical applications of diamond-like carbon coatings: A review, Journal of Biomedical Materials Research Part B: Applied Biomaterials 2007; 83B: 72-84.

[16] Zijian Guo, Xiaolu Pang, Yu Yan, Kewei Gao, Volinsky Alex A, Tong-Yi Zhang, CoCrMo alloy for orthopaedic implant application enhanced corrosion and tribocorrosion properties by nitrogen implantation, Applied Surface Science 2015; 347: 23-34.

[17] Mathew MT, Ariza E, Rocha LA, Vaz F, Fernandes AC, Stack MM, Tribocorrosion behaviour of TiC_xO_y thin films in bio-fluids, Electrochimica Acta 2010; 56: 929-937.

[18] Aldrich-Smith G, Teer DG, Dearnley PA, Corrosion-wear response of sputtered CrN and S-phase coated austenitic stainless steel, Surface and Coatings Technology 1999; 116-119: 1161-1165.

[19] Luo X, Li X, Sun Y, Dong H, Tribocorrosion behavior of S-phase surface engineered medical grade Co–Cr alloy, Wear 2013; 302: 1615-1623.

[20] Bazzoni A, Mischler S, Espallargas N, Tribocorrosion of pulsed plasma-nitrided CoCrMo implant alloy, Tribology Letters 2013; 49: 157-167.

[21] Gabriel Figueiredo Pina C, Dahm KL, Fisher J, Dearnley PA, The damage tolerance of S-phase coated biomedical grade stainless steel, Wear 2007; 263: 1081-1086.

[22] Dearnley PA, Aldrich-Smith G, Corrosion-wear mechanisms of hard coated austenitic 316L stainless steel, Wear 2004; 256: 491-499.

[23] Sun Y, Dearnley PA, Tribocorrosion behavior of duplex S/Cr(N) and S/Cr(C) coatings on CoCrMo alloy in 0.89% NaCl solution, Journal of Bio- and Tribo-Corrosion 2015; 1: 1-13.

[24] Dong H; S-phase surface engineering of Fe–Cr, Co–Cr and Ni–Cr alloys, International Materials Reviews 2010; 55: 65–98.

[25] Sun Y, Production of nitrogen and carbon S phases in austenitic stainless steels by hybrid plasma surface alloying, Surface Engineering 2010; 26: 114-122.

[26] Williams S, Tipper JL, Ingham E, Stone MH, Fisher J, In vitro analysis of the wear, wear debris and biological activity of surface-engineered coatings for use in metal-on-metal total hip replacements, Proceedings of the Institution of Mechanical Engineers Part H-Journal of Engineering in Medicine 2003; 217: 155–163.

[27] Perret J, Boehm-Courjault E, Cantoni M, Mischler S, Beaudouin A, Chitty W, Vernot J-P, EBSD, SEM and FIB characterization of subsurface deformation during tribocorrosion of stainless steel in sulphuric acid, Wear 2010; 269: 383-393.

[28] Dearnley PA, Figueiredo Pina CG, Fisher J, Assessment of S-phase coated medical grade stainless steel (Ortron 90) for use in the human joint replacement corrosion-wear environment, Journal of Physics D: Applied Physics 2008; 41: 105305.

[29] Swaminathan V, Gilbert JL, Potential and frequency effects on fretting corrosion of Ti6Al4V and CoCrMo surfaces, Journal of Biomedical Materials Research Part A 2013; 101: 2602-2612.

[30] Swaminathan V, Zeng H, Lawrynowicz D, Zhang Z, Gilbert JL, Electrochemical investigation of chromium nanocarbide coated Ti-6Al-4V and Co-Cr-Mo alloy substrates, Electrochimica Acta 2012; 59: 387-397.

[31] Sun Y, Vipul Rana, Tribocorrosion behaviour of AISI 304 stainless steel in 0.5 M NaCl solution, Materials Chemistry and Physics 2011; 129: 138-147.

[32] Diomidis N, Celis J-P, Ponthiaux P,Wenger F, Tribocorrosion of stainless steel in sulfuric acid: Identification of corrosion-wear components and effect of contact area, Wear 2010, 269: 93-103

Figure captions:

Fig. 1: A typical ball crater made on the wear track on a duplex coated surface, revealing details of wear depth and deformation behaviour of the multilayer coating in the wear track. The white dashed lines in the upper half of the crater were drawn following the circular contours of the interfaces in the coating-substrate system. The coatings beneath the wear track were deformed beyond the contours into the substrate (white arrows) and the coating at the wear track edges was lifted above the contours (black arrow).

Fig. 2: Evolution of open circuit potential (OCP) with rest time under static condition after cathodic polarization at -600 mV(SCE) for 180 s (a) and anodic polarization curves measured under static condition for the test specimens (b).

Fig. 3: Open circuit potential recorded before, during and after sliding (a) and coefficient of friction (COF) recorded during sliding (b) under open circuit condition. Two representative OCP and COF curves for two different sliding times are presented for each specimen.

Fig. 4: Track profiles measured by profilometer across the corrosion-wear tracks produced on (a) Cr(C)/S coated and (b) Cr(N)/S coated specimens at OCP for various sliding times.

Fig. 5: Microscopic images showing the wear track and a ball crater made on the wear track on the Cr(C)/S coated specimen after corrosion-wear at OCP for (a) 3 h and (b) 6 h. The white dashed lines were drawn following the circular contours of the interfaces in duplex coatings.

Fig. 6: Ball craters made on the wear tracks on the Cr(N)/S coated specimens after sliding at OCP for different times. The white dashed lines were drawn following the circular contours of the interfaces in the duplex coatings. The coatings in the wear track were deformed beyond the contours into the substrate. Deep scratches on the coating surface result in deep deformation of the Cr(N) coating and the S-phase sublayer towards the substrate.

Fig. 7: Microscopic images of the wear tracks on the Cr(N)/S coated specimen after sliding at OCP for various times.

Fig. 8: SEM back scattered images showing surface (a&c) and subsurface (b&d) cracks on the wear track on the Cr(N)/S coated specimen after 6 h (a&b) and 24 h (c&d) sliding. The subsurface cracks in (b) and (d) are observed on the edge of the ball crater made on the wear track. Arrows indicate surface cracks which penetrate through the top Cr(N) coating into the S-phase sublayer. The insert in (c) is the depth profile measured across a blistered area indicated near the lower right-hand corner of the image.

Fig. 9: Total materials loss (TML) in volume as a function of corrosion-wear time at OCP under 2 N load and 60 rpm speed. Single-headed arrows indicate the tests where the top Cr(N) or Cr(C) was worn through and double-headed arrow indicates the test where the S-phase sublayer was worn through.

Fig. 10: Comparison of total material loss resulting from 3 h sliding at CP -700 mV(SCE), at OCP and at AP +100 mV(SCE).

Fig. 11: Ball crater on wear track on Cr(C)/S coated specimen produced by sliding at (a) -700 mV(SCE) and (b)100 mV(SCE), at 2 N load for 3 h.

Fig. 12: Optical microscopic (a) and SEM (b) images showing the surface morphology of the wear track on Cr(N)/S coated specimen produced at the anodic potential 100 mV(SCE), at 2 N load for 3 h.

Fig. 13: Ball crater made on the wear track on Cr(N)/S coated specimen produced at (a) -700 mV(SCE) and (b) 100 mV(SCE), at 2 N load for 3 h. After abrading away the Cr(N) coating and the S-phase sublayer, the pit initially seen on the wear track surface produced at 100 mV(SCE) can be clearly seen deep into the substrate.

Fig. 14: Enlarged view of the ball carter on the wear track shown in Fig. 13b. Most of the cracks continue from the wear surface through the Cr(N) coating into the S-phase sublayer to reach the substrate.

Fig. 15: Anodic currents measured before, during and after sliding at anodic potential of 100 mV(SCE). Note the increase in current from the Cr(N)/S coated specimen after the termination of sliding.

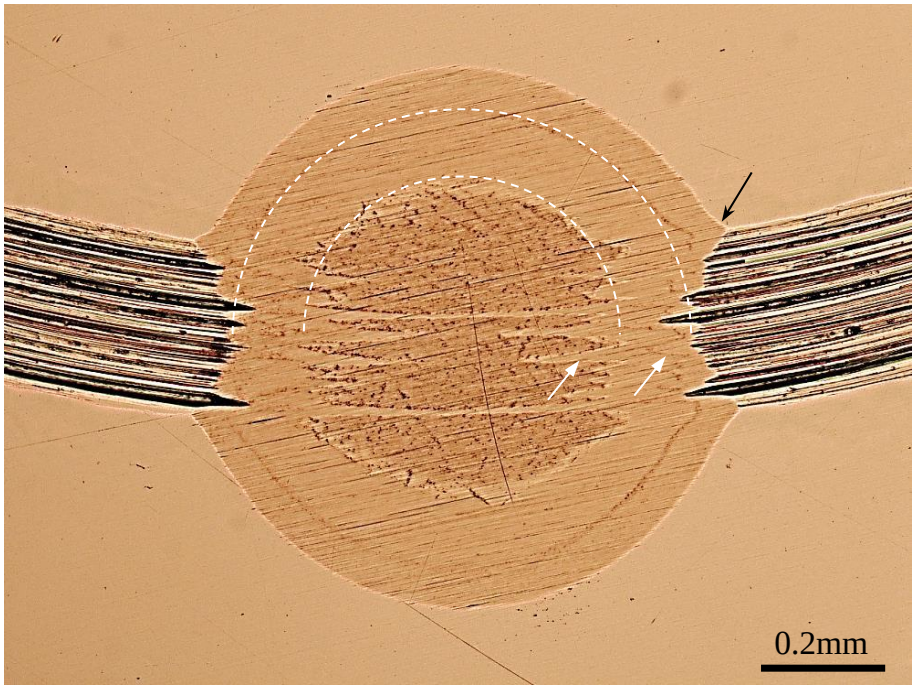

Fig. 1: A typical ball crater made on the wear track on a duplex coated surface, revealing details of wear depth and deformation behaviour of the multilayer coating in the wear track. The white dashed lines in the upper half of the crater were drawn following the circular contours of the interfaces in the coating-substrate system. The coatings beneath the wear track were deformed beyond the contours into the substrate (white arrows) and the coating at the wear track edges was lifted above the contours (black arrow).

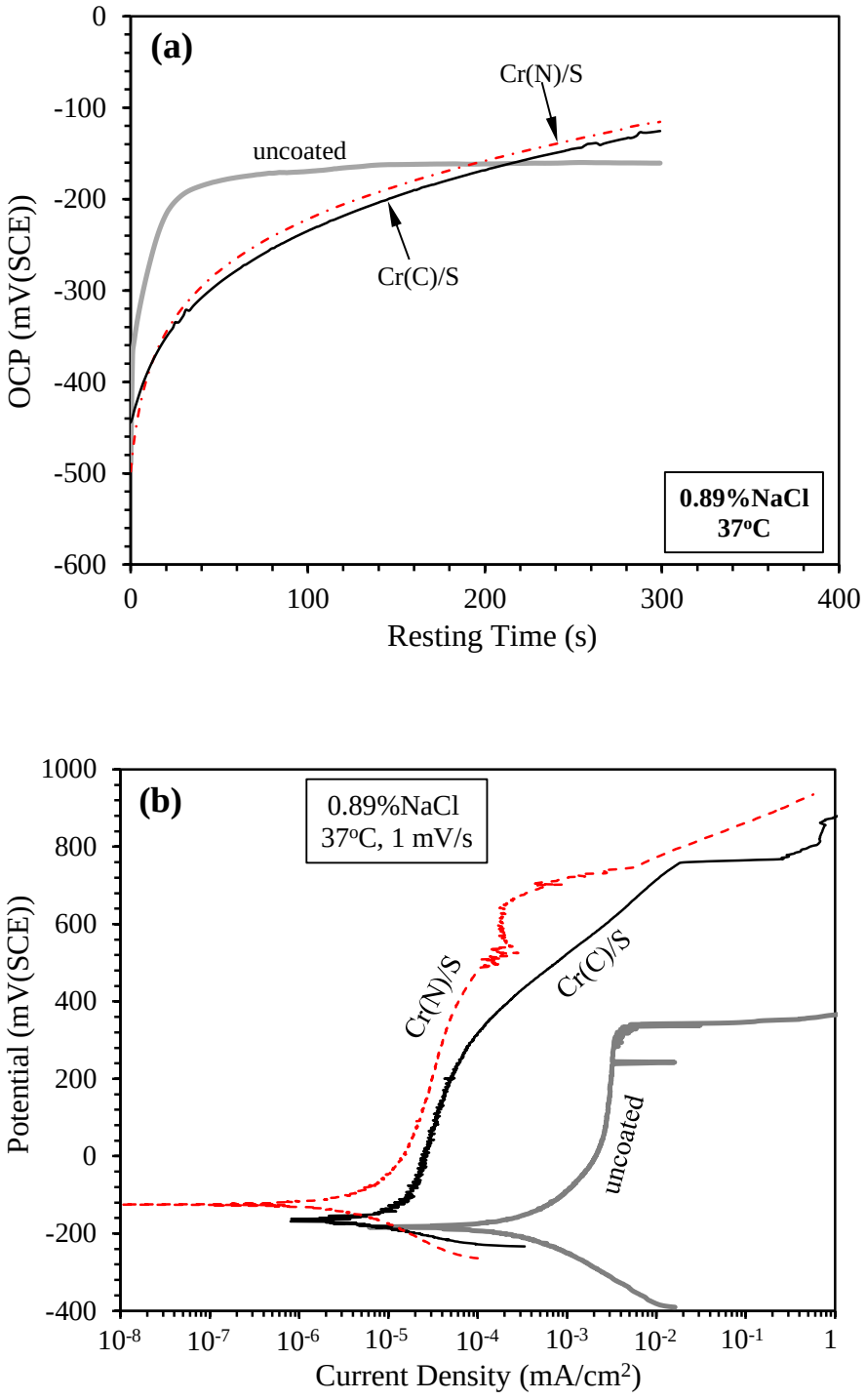

Fig. 2: Evolution of open circuit potential (OCP) with rest time under static condition after cathodic polarization at -600 mV(SCE) for 180 s (a) and anodic polarization curves measured under static condition for the test specimens (b).

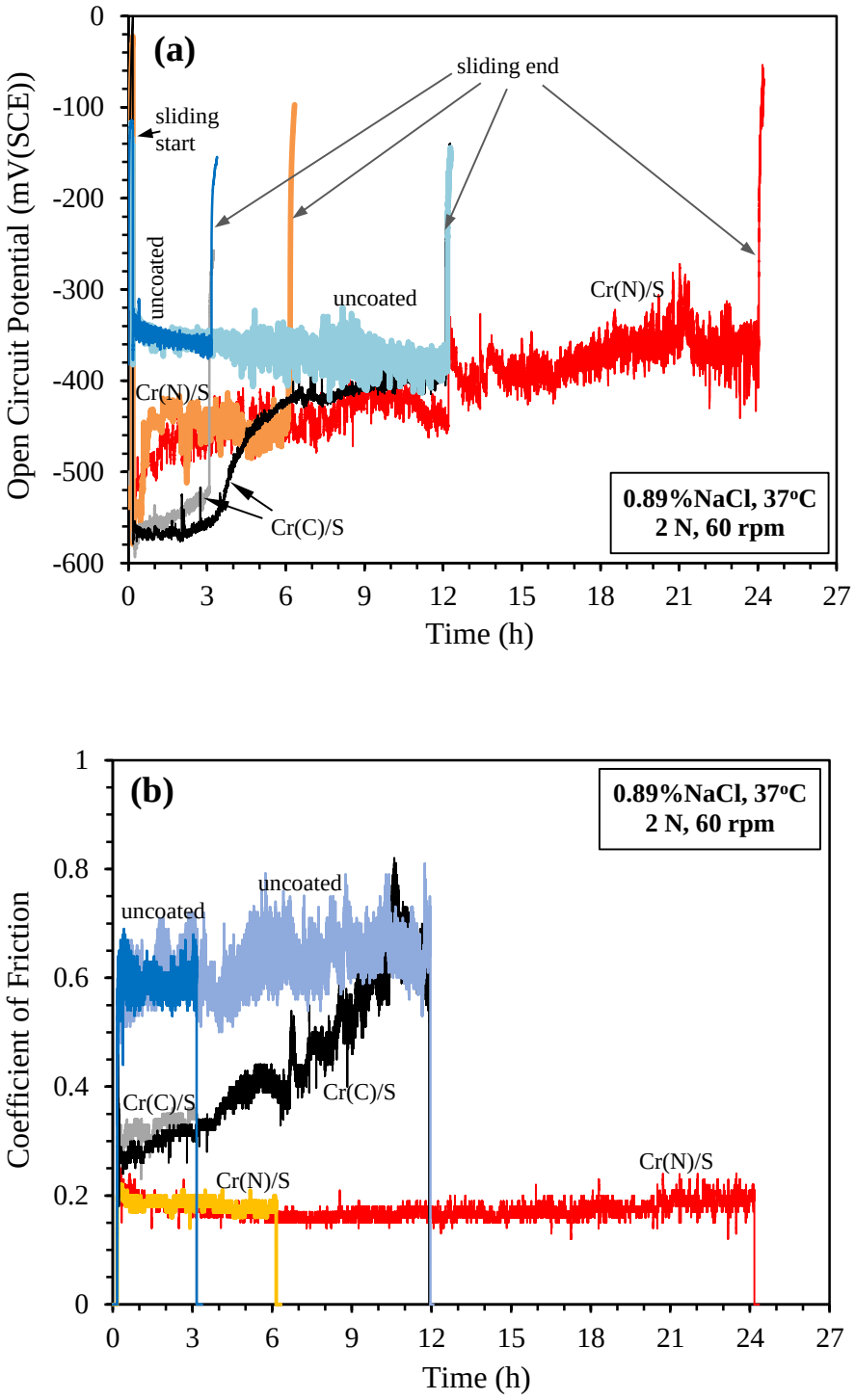

Fig. 3: Open circuit potential recorded before, during and after sliding (a) and coefficient of friction (COF) recorded during sliding (b) under open circuit condition. Two representative OCP and COF curves for two different sliding times are presented for each specimen.

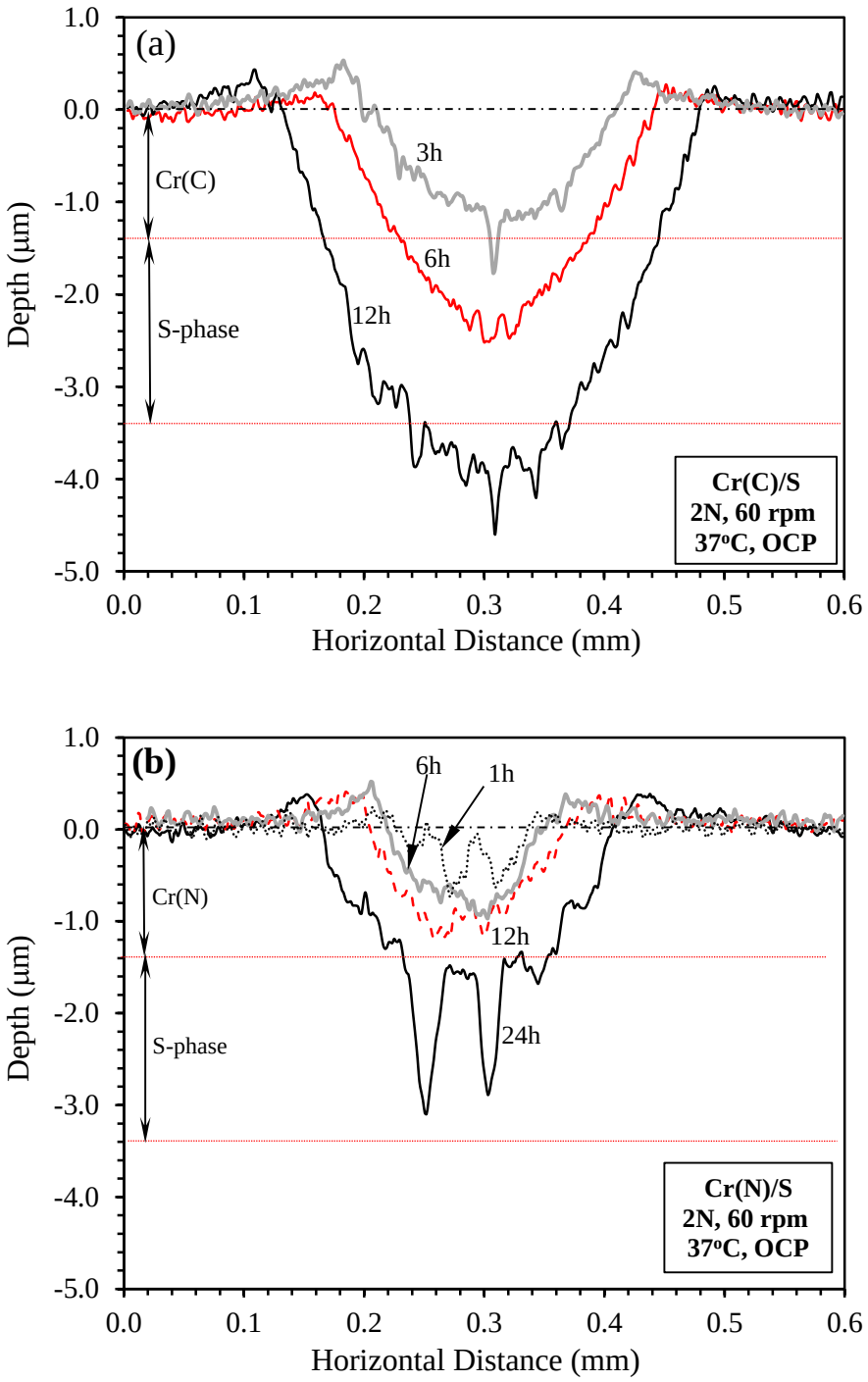

Fig. 4: Track profiles measured by profilometer across the corrosion-wear tracks produced on (a) Cr(C)/S coated and (b) Cr(N)/S coated specimens at OCP for various sliding times.

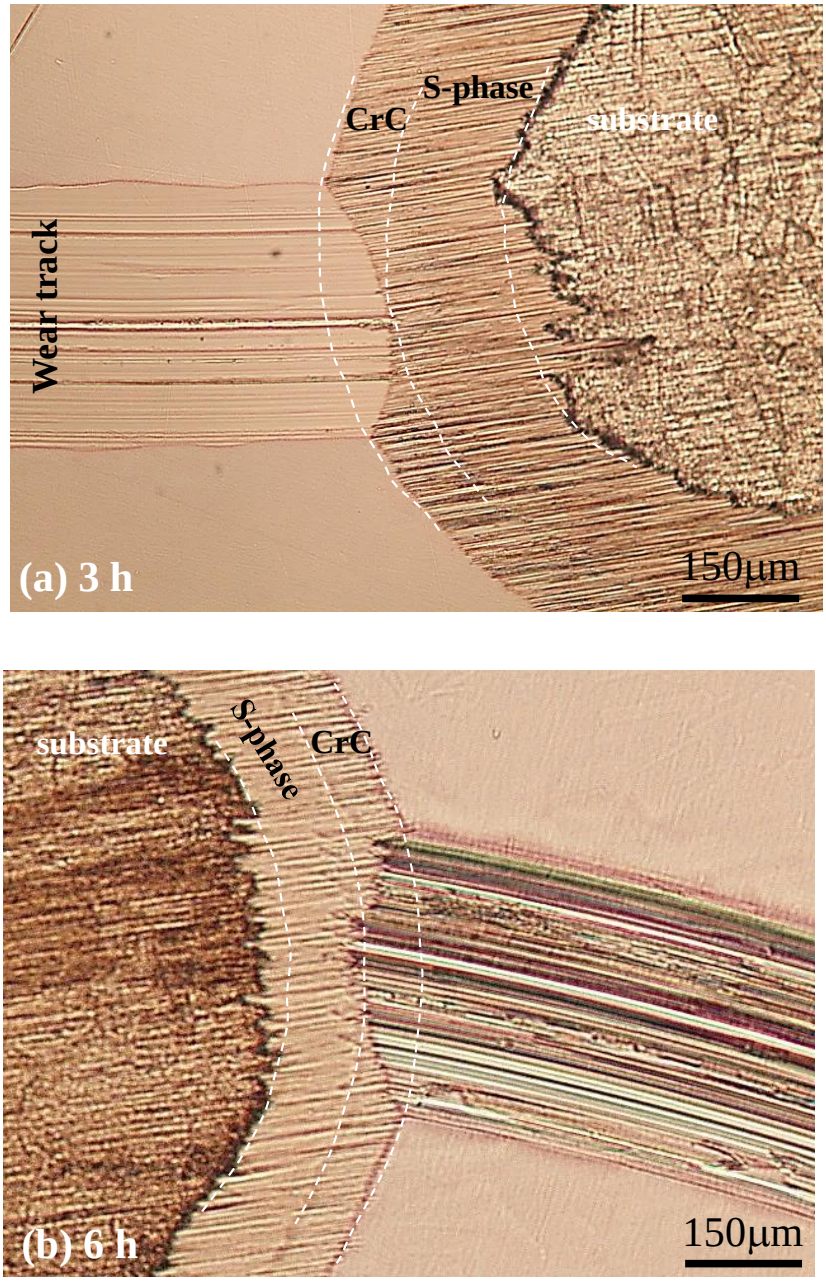

Fig. 5: Microscopic images showing the wear track and a ball crater made on the wear track on the Cr(C)/S coated specimen after corrosion-wear at OCP for (a) 3 h and (b) 6 h. The white dashed lines were drawn following the circular contours of the interfaces in duplex coatings.

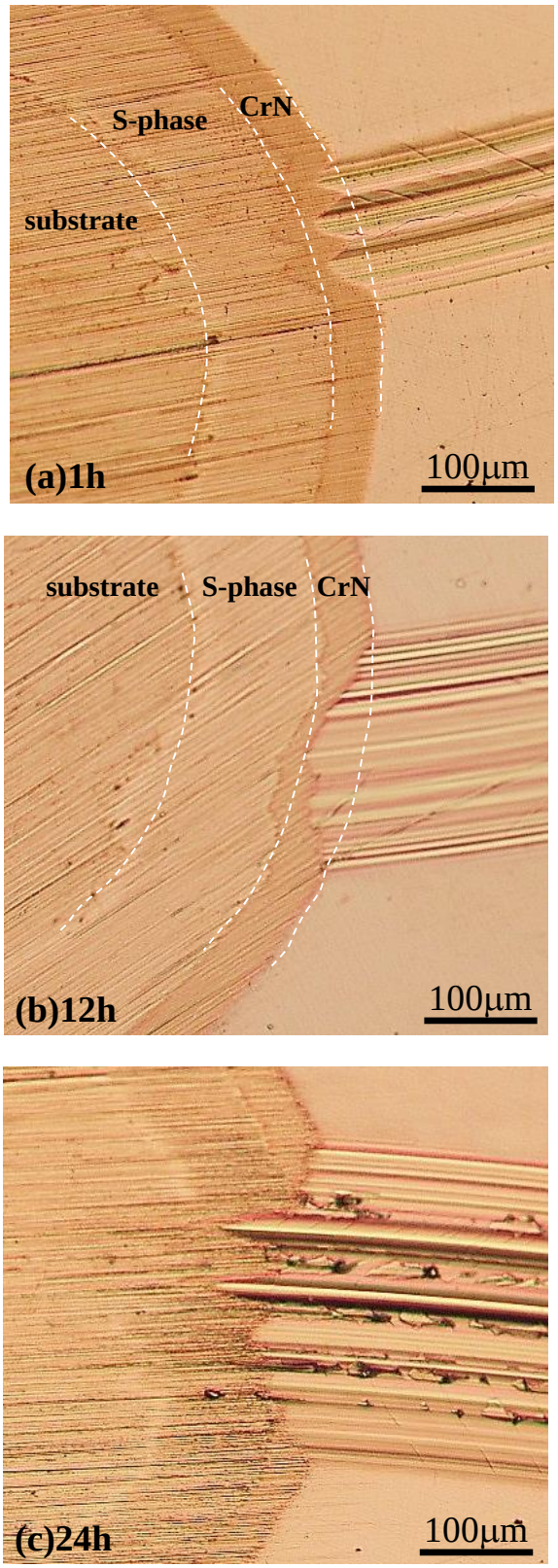

Fig. 6: Ball craters made on the wear tracks on the Cr(N)/S coated specimens after sliding at OCP for different times. The white dashed lines were drawn following the circular contours of the interfaces in the duplex coatings. The coatings in the wear track were deformed beyond the contours into the substrate. Deep scratches on the coating surface result in deep deformation of the Cr(N) coating and the S-phase sublayer towards the substrate.

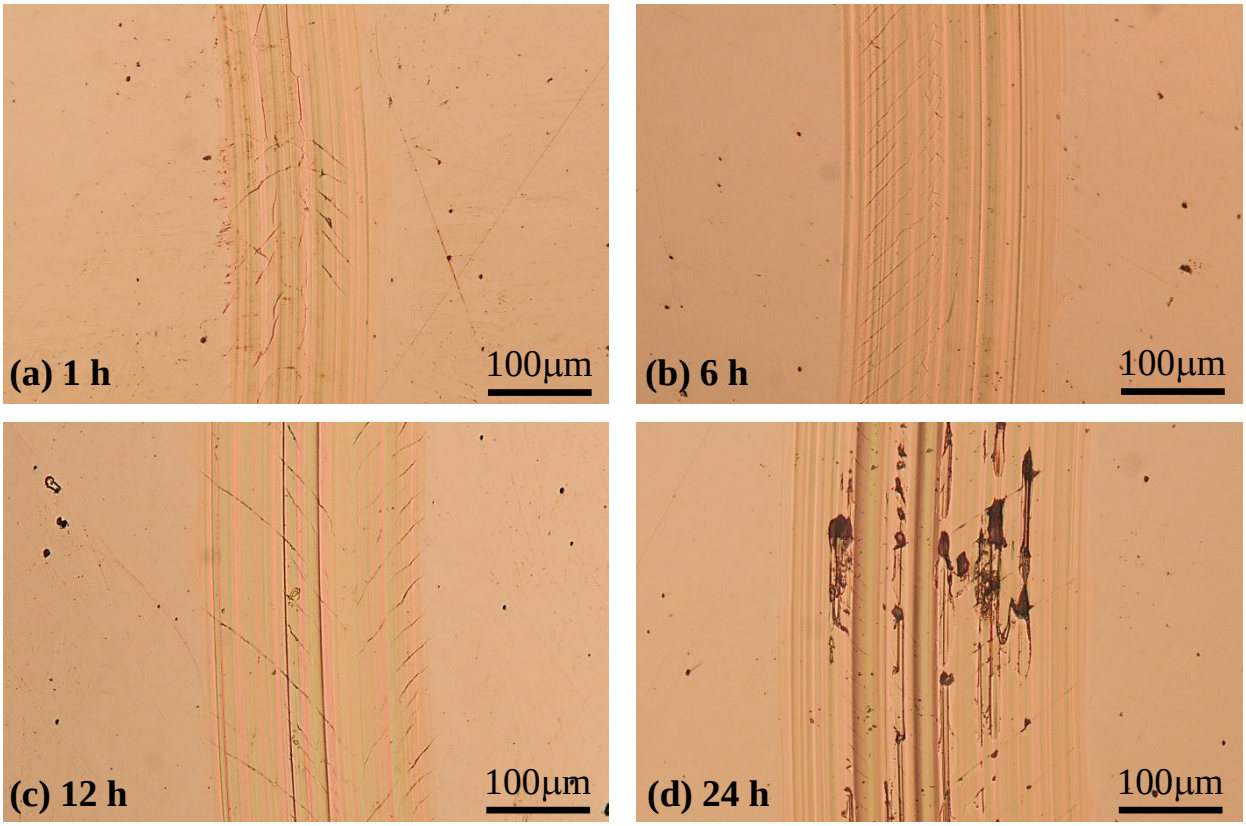

Fig. 7: Microscopic images of the wear tracks on the Cr(N)/S coated specimen after sliding at OCP for various times.

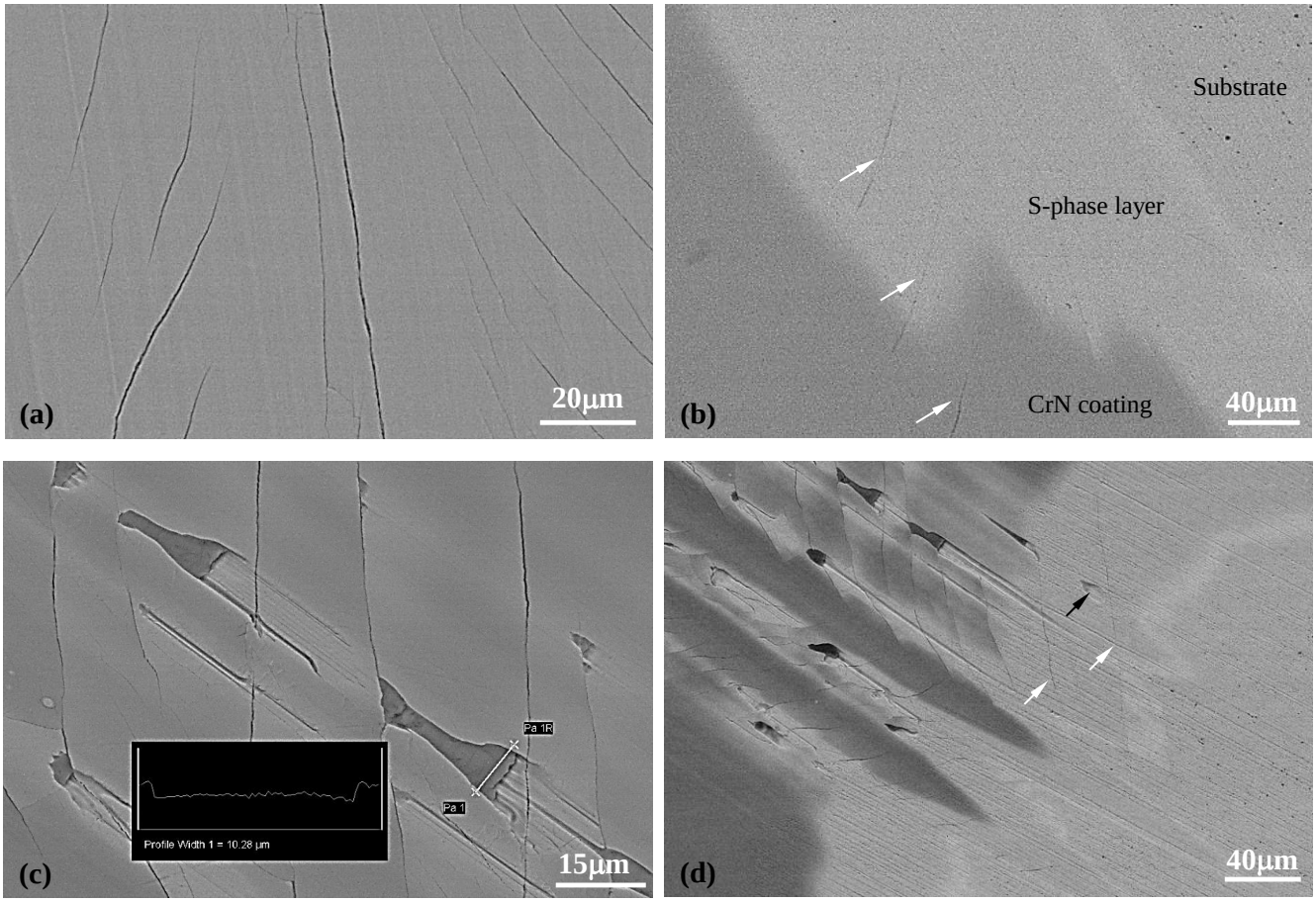

Fig. 8: SEM back scattered images showing surface (a&c) and subsurface (b&d) cracks on the wear track on the Cr(N)/S coated specimen after 6 h (a&b) and 24 h (c&d) sliding. The subsurface cracks in (b) and (d) are observed on the edge of the ball crater made on the wear track. Arrows indicate surface cracks which penetrate through the top Cr(N) coating into the S-phase sublayer. The insert in (c) is the depth profile measured across a blistered area indicated near the lower right-hand corner of the image.

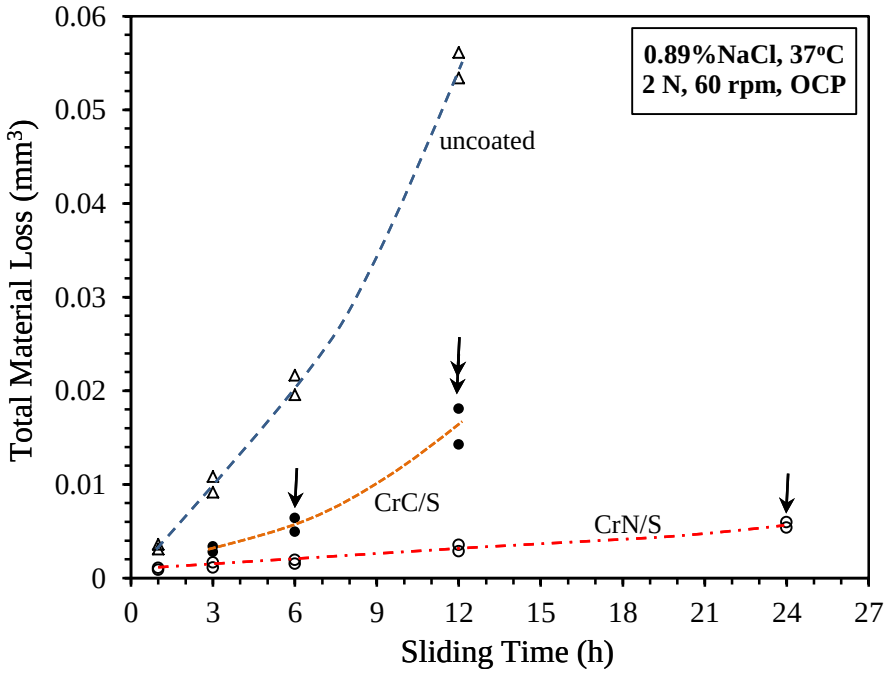

Fig. 9: Total materials loss (TML) in volume as a function of corrosion-wear time at OCP under 2 N load and 60 rpm speed. Single-headed arrows indicate the tests where the top Cr(N) or Cr(C) was worn through and double-headed arrow indicates the test where the S-phase sublayer was worn through.

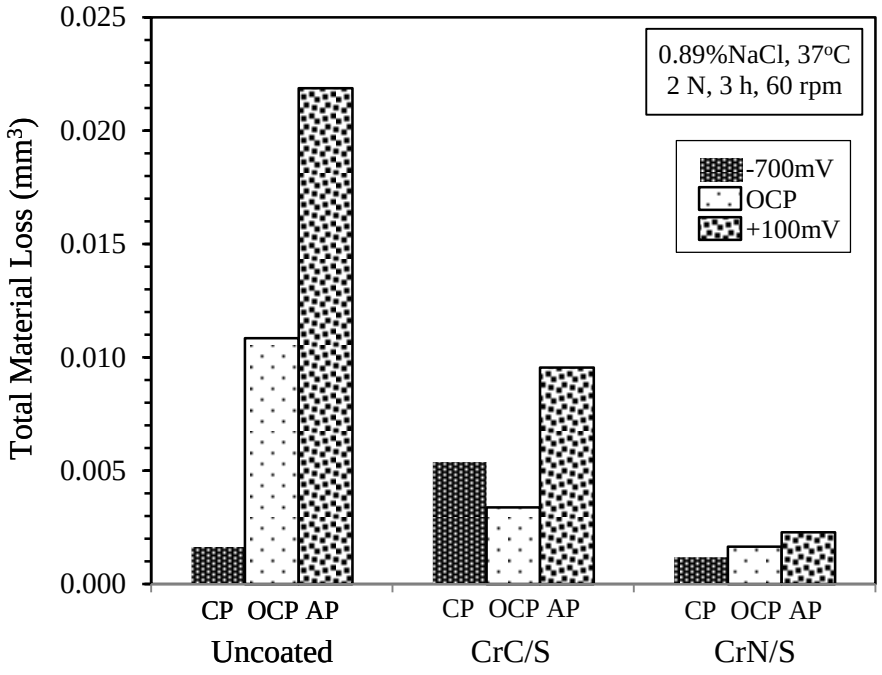

Fig. 10: Comparison of total material loss resulting from 3 h sliding at CP -700 mV(SCE), at OCP and at AP +100 mV(SCE).

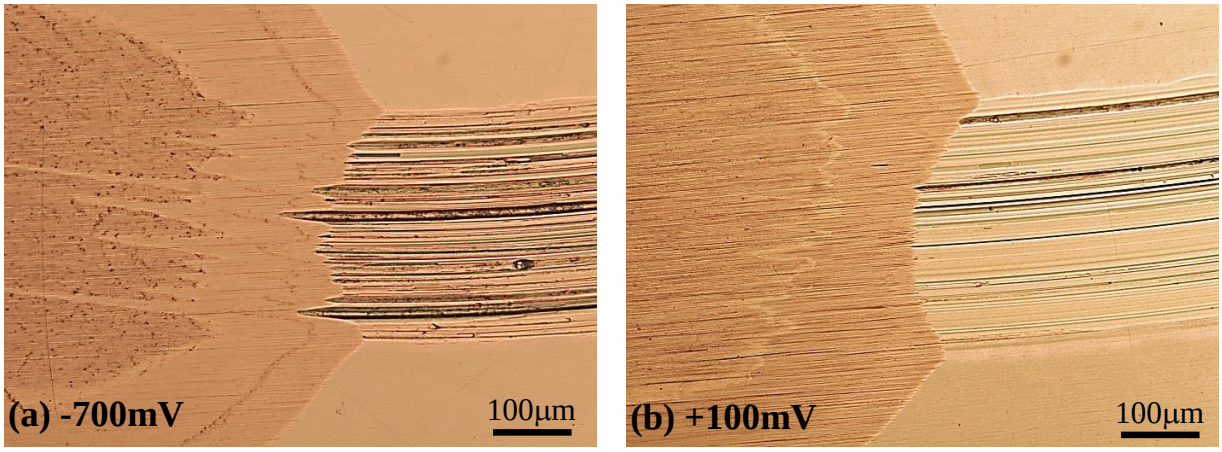

Fig. 11: Ball crater on wear track on Cr(C)/S coated specimen produced by sliding at (a) -700 mV(SCE) and (b)100 mV(SCE), at 2 N load for 3 h.

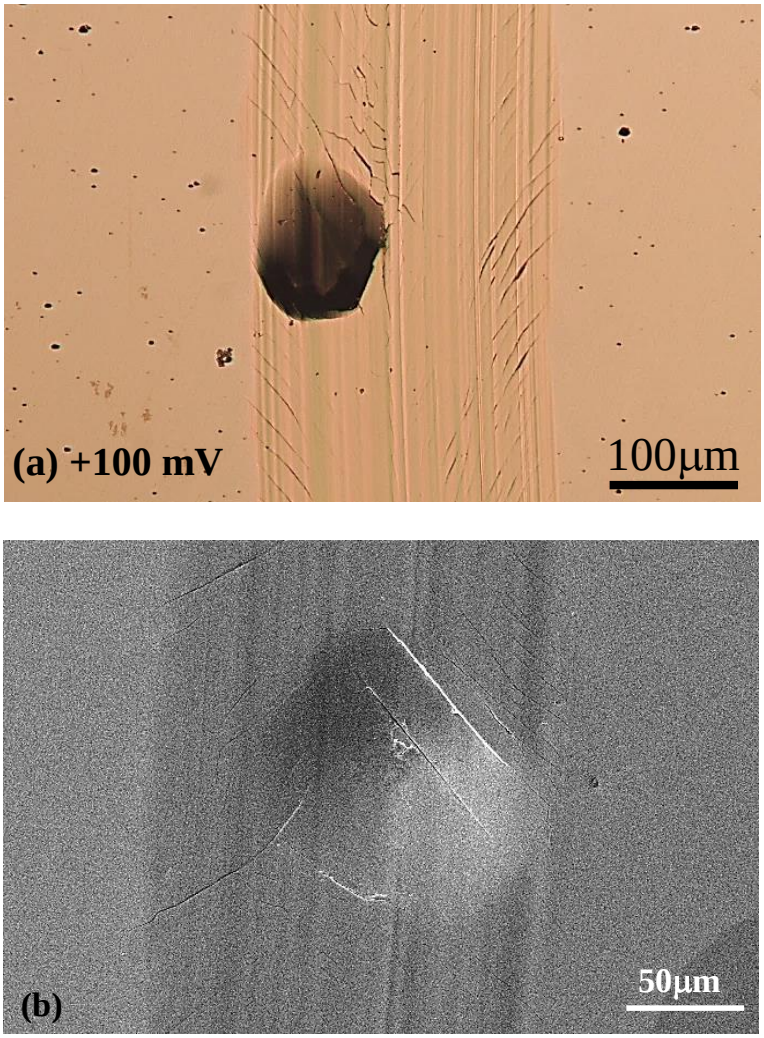

Fig. 12: Optical microscopic (a) and SEM (b) images showing the surface morphology of the wear track on Cr(N)/S coated specimen produced at the anodic potential 100 mV(SCE), at 2 N load for 3 h.

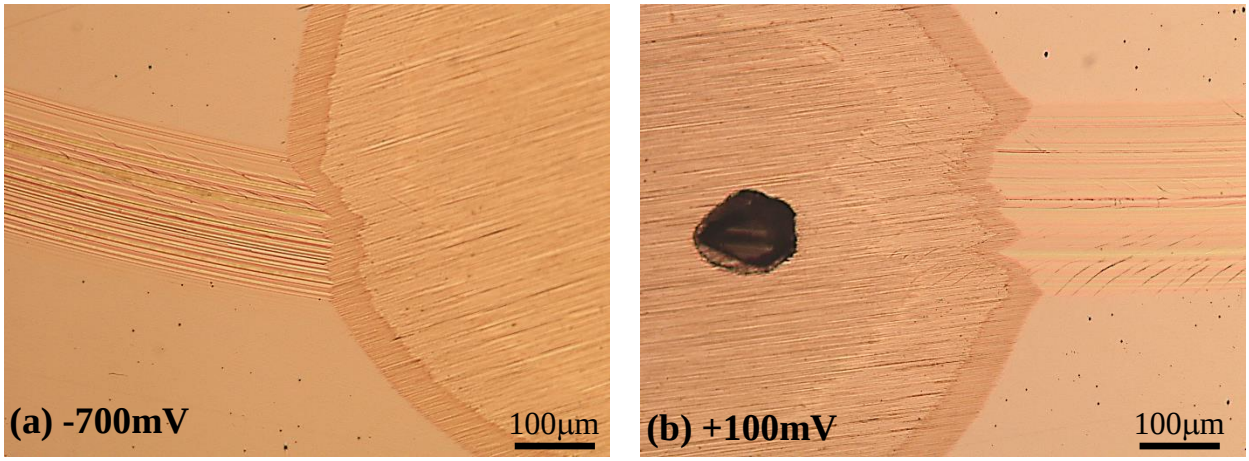

Fig. 13: Ball crater made on the wear track on Cr(N)/S coated specimen produced at (a) -700 mV(SCE) and (b) 100 mV(SCE), at 2 N load for 3 h. After abrading away the Cr(N) coating and the S-phase sublayer, the pit initially seen on the wear track surface produced at 100 mV(SCE) can be clearly seen deep into the substrate.

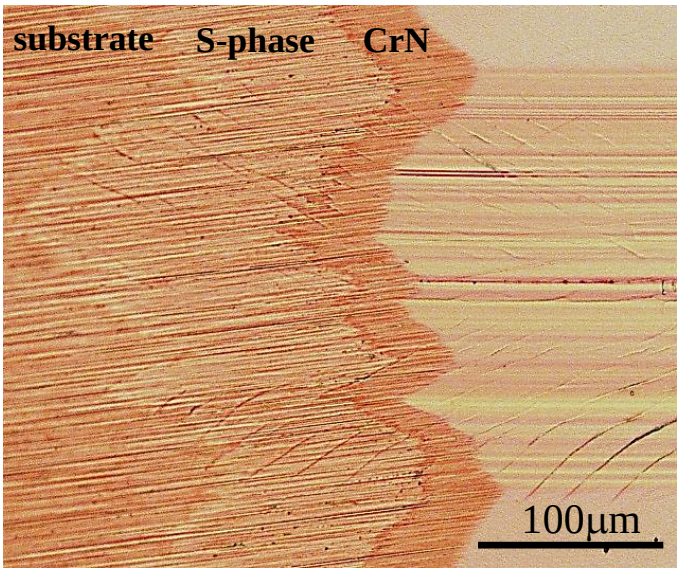

Fig. 14: Enlarged view of the ball carter on the wear track shown in Fig. 13b. Most of the cracks continue from the wear surface through the Cr(N) coating into the S-phase sublayer to reach the substrate.

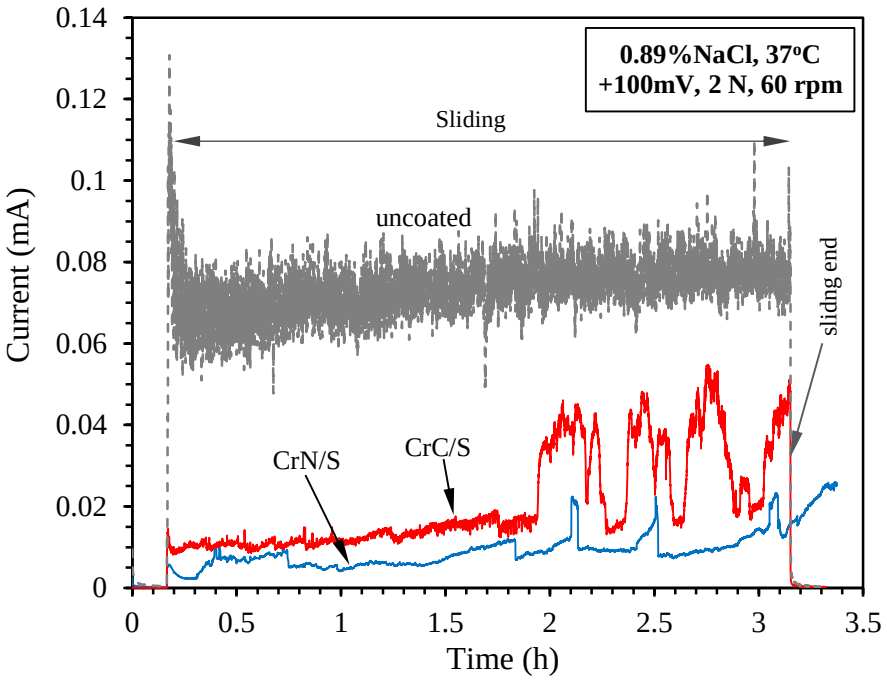

Fig. 15: Anodic currents measured before, during and after sliding at anodic potential of 100 mV(SCE). Note the increase in current from the Cr(N)/S coated specimen after the termination of sliding.